Letter

$BaFe_2S_3$: A quasiunidimensional noncentrosymmetric superconductor

S. Deng [1,*] A. Roll [2,3,*] W. G. Zheng [2,*] G. Giri [1,†] T. Vasina [1] D. Bounoua [3] P. Fertey [4] M. Verseils [4] C. Bellin [5] A. Forget [6] D. Colson [6] P. Foury-Leylekian [2] M. B. Lepetit [1,7] and V. Balédent [2,8,‡]

[1] *Institut Laue Langevin, 71 avenue des Martyrs, 38042 Grenoble, France*

[2] *Université Paris-Saclay, CNRS, Laboratoire de Physique des Solides, 91405 Orsay, France*

[3] *Université Paris-Saclay, CNRS-CEA, Laboratoire Léon Brillouin, 91191 Gif sur Yvette, France*

[4] *Synchrotron SOLEIL, L'Orme des Merisiers, Saint Aubin BP 48, 91192 Gif-sur-Yvette, France*

[5] *Université Pierre et Marie Curie, IMPMC, CNRS UMR7590, 4 Place Jussieu, 75005 Paris, France*

[6] *Université Paris-Saclay, CEA, CNRS, SPEC, 91191 Gif-sur-Yvette, France*

[7] *Institut Néel, CNRS, 38042 Grenoble, France*

[8] *Institut Universitaire de France (IUF)*

(Received 3 March 2025; revised 1 February 2026; accepted 10 February 2026; published 16 March 2026)

Introduction. The spin-ladder compounds of the $BaFe_2X_3$ (X = chalcogen) family may be viewed as dimensional reductions—along stripelike motifs—of the two-dimensional iron-based pnictide planes extensively studied since 2006. Remarkably, despite their reduced dimensionality, these materials retain the capacity for unconventional ground states, exemplified by the emergence of superconductivity in $BaFe_2Se_3$ under applied pressure beyond 10 GPa, following a structural phase transition at 4 GPa. Here, we report a comprehensive investigation combining high-resolution single-crystal x-ray diffraction, infrared spectroscopy, and *ab initio* calculations, which together elucidate the true crystallographic nature of this pressure-induced superconducting phase. While x-ray diffraction alone reveals a symmetry lowering from the widely accepted orthorhombic *Cmcm* group to a monoclinic structure, it lacks sufficient sensitivity to resolve the precise space group. By integrating vibrational spectroscopy with density functional theory, we provide unambiguous evidence that the high-pressure phase is noncentrosymmetric, adopting the polar space group $P2_1$. These findings not only revise the structural assignment of $BaFe_2Se_3$ in its superconducting state, but also establish its noncentrosymmetric character—an essential ingredient for potential unconventional pairing mechanisms—thereby opening different perspectives on the interplay between lattice symmetry, dimensionality, and superconductivity in iron-based materials.

DOI: 10.1103/jzt8-3t2c

Unconventional superconductivity remains one of the most emblematic quantum properties in solid-state physics, resisting any consensus on a phenomenological or microscopic model [1–3]. Initiated by the discovery of high-critical temperature cuprates, this pursuit of elevated temperatures has led to the exploration of new materials such as iron-based pnictides, heavy fermion compounds, and, more recently, nickelates [4]. While the mechanism behind Cooper pair formation in these families remains elusive, there is a broad consensus that understanding superconductivity requires investigating phases and orders neighboring the superconducting dome [5,6]. Indeed, to elucidate pairing mechanisms or test proposed models, it is pertinent to observe the presence of competing or intertwined order parameters. This has been done in particular in numerous quasi-two-dimensional (2D) iron-based superconductors such as FeSe or $BaFe_2As_2$, whose square-lattice planes and layered architectures have been extensively studied both structurally and magnetically [4,7–10]. These studies have revealed how structural and magnetic degrees of freedom, often intimately linked, evolve upon approaching the superconducting dome via chemical doping or applied pressure. Recently, new spin-ladder iron-based systems have demonstrated superconductivity under pressure. With a general formula of $BaFe_2X_3$ (X=S and Se), they represent the first quasi-one-dimensional iron-based superconductors devoid of a square-lattice motif [11,12]. The quasi-one-dimensional character of these compounds originates from their two-leg ladder crystal structure and is reflected in strongly anisotropic transport properties and low-dimensional magnetic correlations [12–15]. In this context, these two compounds offer a unique opportunity to investigate how reducing dimensionality from 2D to 1D affects the delicate balance between magnetism, structure, and superconductivity.

Consisting of two iron ladders per unit cell, the $BaFe_2Se_3$ and $BaFe_2S_3$ compounds were respectively reported to crystallize in the *Pnma* and *Cmcm* space groups [16]. In the *Cmcm* structure, the ladders, formed by edge-sharing FeX_4 tetrahedra along the c axis, are perfectly contained in the (a, c) plane, whereas a tilt is observed in *Pnma*. Interestingly, $BaFe_2Se_3$ is reported to undergo a transition from *Pnma* to *Cmcm* above 3 to 4 GPa [17], suggesting a common atomic structure between the two compounds close to the superconducting phase. This apparent universality of the neighboring phases

*These authors contributed equally to this work.

†Present address: Physics Department, VIT Bhopal University, Bhopal, India.

‡Contact author: victor.baledent@universite-paris-saclay.fr

of the superconducting dome is reinforced by the presence of the same magnetic order, as measured by neutron diffraction under pressure [18]. However, a more thorough investigation of single crystals of $BaFe_2Se_3$, utilizing x-ray diffraction, infrared spectroscopy, and *ab initio* calculations, revealed that the actual space group at ambient pressure is *Pm*, a significantly lower symmetry than the previously reported average *Pnma* space group [19,20]. Understanding the symmetries at play in these compounds is therefore crucial for comprehending their physical properties, especially since such symmetry breaking can endow $BaFe_2Se_3$ with multiferroic behavior. An even more intriguing possibility is that the loss of inversion symmetry persists into the superconducting phase, placing $BaFe_2Se_3$ within the rare class of noncentrosymmetric superconductors [21–23].

Until now, very limited information has been available regarding the crystallographic structure of the superconducting phase itself, despite its crucial importance for understanding the nature of superconductivity in this system. In light of the ambient-pressure results, it is therefore essential to investigate the structure of $BaFe_2Se_3$ in single crystals under combined high-pressure and low-temperature conditions. In this Letter, we present a study of $BaFe_2Se_3$ under pressure, combining x-ray diffraction (XRD), infrared (IR) and Raman spectroscopies, and *ab initio* calculations. Our results reveal that the high-pressure space group of $BaFe_2Se_3$ in the phase where superconductivity emerges is $P2_1$. This symmetry establishes $BaFe_2Se_3$ as one of the very few known examples of a quasi-one-dimensional noncentrosymmetric superconductor.

Experimental methods. Single crystals of $BaFe_2Se_3$ were grown using the self-flux method as described in Ref. [19]. We emphasize that the samples used in this study originate from the same batch that was extensively characterized in previous works. Compositional uniformity was verified by energy-dispersive x-ray spectroscopy (EDX), showing a nominal stoichiometry within 2% uncertainty (see the Supplemental Material of Ref. [19]), and scanning electron microscopy (SEM) confirmed the absence of structural defects at the microscale [24]. Although structural symmetry, particularly noncentrosymmetry, can be sensitive to stoichiometry and sample quality, no deviation from the reported superconducting composition or structure was detected. Despite the absence of low-temperature resistivity measurements under pressure showing superconductivity, we are confident that the observed noncentrosymmetric structure corresponds to a superconducting phase representative of this material family. For each experiment, one or several single crystals of $BaFe_2Se_3$ were loaded in a membrane-driven diamond anvil cell (DAC), using a stainless steel gasket with pressure transmitting media adapted to each technique (see details in the Supplemental Material (SM) [25], and Refs. [26,27] therein). The pressure inside the diamond anvil cell was measured using the ruby fluorescence technique, yielding a 5% relative accuracy on the pressure value [28]. XRD and IR reflectivity were performed on the CRISTAL and AILES beam line, respectively, at synchrotron SOLEIL. Due to technical constraints associated with the cryostat used for measurements in diamond anvil cells required for high-pressure experiments, the lowest temperatures achieved were not identical across techniques: 10 K for diffraction measurements and 50 K for infrared spectroscopy. However, as shown in our previous work at ambient pressure [20], phonon energies exhibit minimal variation between 50 and 10 K.

Raman scattering experiments were performed at IMPMC (Paris) using a 534 nm laser source with a fixed power of 80 mW in a backscattering geometry. Measurements were carried out at 300 K, as the Raman signal is particularly weak in this family of compounds already at ambiant conditions, consistent with previous reports [29], preventing us from measuring at both low temperature and high pressure despite several attempts. Polarized Raman spectra were successfully measured under pressure using well-defined scattering geometries, expressed in Porto notation as (a, a) and (c, c) configurations, where both incident and scattered electric fields are aligned along the crystallographic **a** and **c** directions, respectively (in *Cmcm* notation).

The *ab initio* calculations were done using density functional theory (DFT). In order to best account for the eletronic correlation at the Fermi level, we used the hybrid B3LYP functional [30] and a localized basis set. An atomic Gaussian basis of $3\zeta + P$ quality was used for the Fe and Se atoms [31]. The Ba atoms were represented using a relativistic core pseudopotential of the Stuttgard group [32] and the associated basis set where the diffuse functions exponents were taken as 1.2, as recommended by Scuseria *et al.* [33]. The calculations were done using the CRYSTAL23 code [34]. The shrinking factor was set to $8 \times 12 \times 4$, resulting in a sampling net of 126 **k** points. The stripe spin ordering found in neutron scattering experiments of $BaFe_2Se_3$ under pressure [18] was used in all calculations.

X-ray diffraction. The most comprehensive study of structural properties in this compound is provided in Ref. [17], where room-temperature x-ray data under pressure up to 50 GPa are provided. Between 0 and 3.5 GPa, Svitlyk *et al.* propose a *Pnma* space group; between 3.5 and 16.6 GPa, a *Cmcm* group; and above 16.6 GPa, an isostructural *Cmcm* phase where the **b** axis collapses while the **a** and **c** ones expand [17].

One should, however, remember that in these compounds, diffraction measurements often lead to average structures, rather than true space groups. Indeed, while at ambient pressure x-ray results were suggesting a *Pnma* group [16,17], our high-resolution x-ray and lattice dynamic investigations clearly identified small symmetry breakings and the true space group to be *Pm*.

We collected thousands of Bragg reflections at selected pressure and temperature values; see details in the SM [25].

At 300 K, above the 3 to 4 GPa transition and up to 12 GPa, our x-ray data confirm the reported [17] *Cmcm* space group, as we observed no intensity on forbidden reflections [see Fig. 1(b)].

At 10 K, the data collected at 5 and 12 GPa indicate that the space group cannot be *Cmcm*. Specifically, we observed intensities for (i) $H + K$ odd, even for $L = 0$, indicating a break in C centering and of the $\{m_{00z}, \frac{1}{2}\frac{1}{2}\frac{1}{2}\}$ glide mirror; (ii) $(H, 0, L)$ with L odd indicating a breaking of the **c** glide mirror perpendicular to the **b** axis; (iii) no intensity on the $(0, 0, L)$ with L odd peaks; and (iv) a clear monoclinic structure with a significant angle $\approx 103^\circ$ and the unique axis along the **c** axis of the *Cmcm*. As a consequence, the space group for $BaFe_2Se_3$

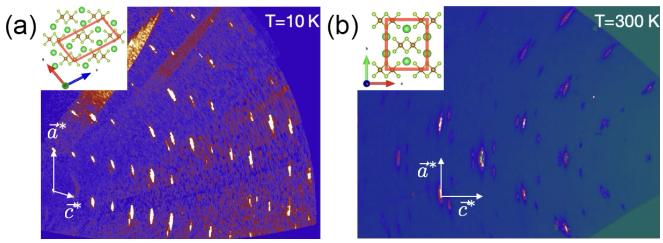

FIG. 1. Reconstructions of the reciprocal space at 12 GPa, (a) at low temperature in the (H,0,L) plane perpendicular to the ladders in the monoclinic setting and (b) at ambiant temperature in the (H,K,0) plane perpendicular to the ladders in the *Cmcm* setting. Insets show the lattice unit in red with the direct lattice vectors in their respective settings.

at high pressure and low temperature should be either $P2_1/m$ or $P2_1$, with the unique axis along the **c** axis of the *Cmcm* (see the SM [25] for a detailed symmetry analysis).

We refined the structure for both space groups using JANA software [35]. The refined structures at 5 and 12 GPa at 10 K, in the superconducting phase, are reported in the SM [25]. The refinements yielded similar results for both space groups, with agreement factor values (R_{obs}) of 6.81 ($P2_1/m$) and 6.33 ($P2_1$) at 5 GPa, and 3.77 ($P2_1/m$) and 3.76 ($P2_1$) at 12 GPa (see the SM [25] for details). Although R_{obs} is marginally better for the $P2_1$ space group, the difference is within the margin of uncertainty, making it unreasonable to definitively assert this space group as the actual space group based on these grounds alone. To resolve this ambiguity, we performed geometry optimization using DFT. However, similarly to XRD, it was impossible to conclude as no significant energy lowering was observed in the $P2_1$ group. We then examined the lattice dynamics using infrared and Raman spectroscopy, comparing the results with *ab initio* calculations.

Lattice dynamics. We measured the pressure evolution of the IR reflectivity at 50 K for two configurations of the incident polarization: with the electric field aligned along the **a** or **c** direction (in *Cmcm* notation). In the centrosymmetric *Cmcm* phase, infrared-active phonons transform according to the B_{1u}, B_{2u}, and B_{3u} irreducible representations. Within the conventional *Cmcm* setting, these modes are associated with electric fields polarized along **c** (B_{1u}), **b** (B_{2u}), and **a** (B_{3u}), respectively. As a consequence, our infrared measurements probe only the B_{1u} modes for **E** ∥ **c** and the B_{3u} modes for **E** ∥ **a**, while the B_{2u} modes polarized along **b** are not accessible in our experimental geometry.

At low pressure, we resolved the phonons previously published [20] and observed the expected hardening under pressure up to 4 GPa. It was associated with a decrease in amplitude, likely due to the progressive metallization already reported [12].

Above the 4 GPa transition, there is a substantial increase in the optical conductivity, resulting in an elevated baseline for the reflectivity, making it a challenge to discern the phonons. Consequently, only the most intense phonons remain visible and can be fitted. In Figs. 2(a) and 2(c), we present a map of the reflectivity evolution as a function of pressure, to facilitate the visualization of the phonons and their pressure-induced changes. This approach helps distinguishing phonons from

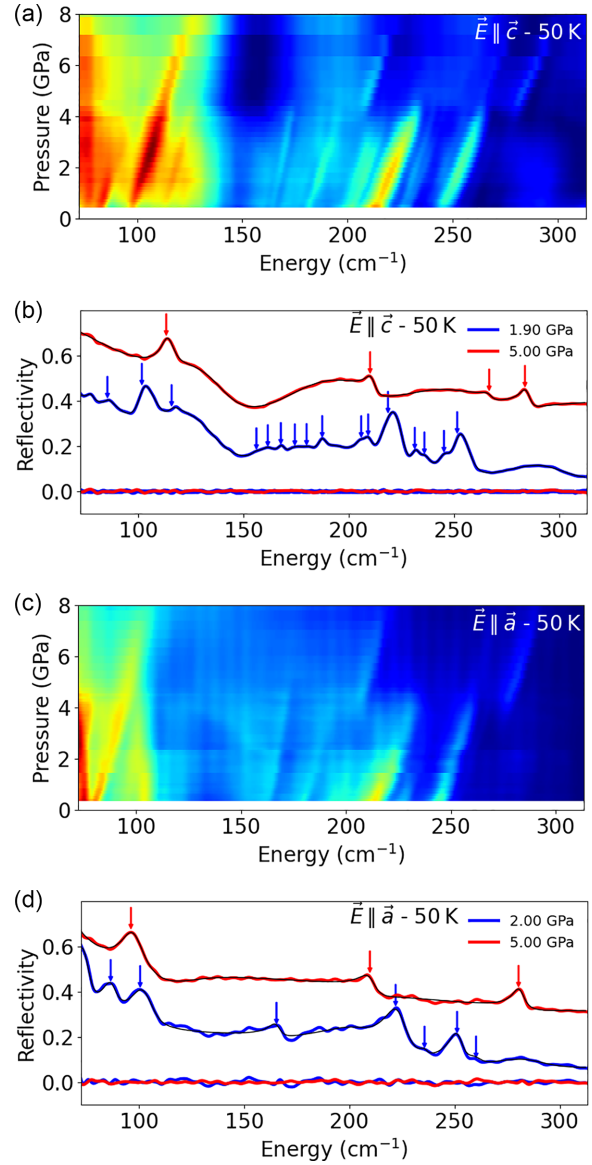

FIG. 2. (a),(c) Reflectivity of $BaFe_2Se_3$ as a function of energy and pressure for **E** ∥ **c** (B_{1u}) and **E** ∥ **a** (B_{3u}) in the *Cmcm* setting, respectively. The value of the reflectivity at 310 cm^{-1} has been subtracted to remove the baseline shift due to progressive metallization. (b),(d) Selected reflectivity at 2 GPa (blue line) and 5 GPa (red line) for both polarizations. The fit of the reflectivity is represented by the black line, and the difference between the data and the fit is shown in the corresponding color. Arrows indicate the positions of the fitted phonons.

baseline oscillations. The phonons shift in energy with pressure, while the experimental artifacts, such as oscillations, remain at the same energy.

In Figs. 2(b) and 2(d), we depict the reflectivity at 2 and 5 GPa for both polarizations, fitted with the standard Drude-Lorentz model, where the dielectric function is expressed as the sum of harmonic oscillators [20]. The extracted phonon frequencies are reported in Table I for the 2 and 5 GPa measurements.

At low temperature and high pressure, where the monoclinic symmetry is stabilized, the possible centrosymmetric

TABLE I. Frequencies (cm^{-1}) of optical phonons in the $P2_1/m$ and $P2_1$ space groups, obtained from DFT calculations and IR measurements at 50 K. Only the DFT modes with frequencies above 80 cm^{-1} are listed. See the SM [25] for a complete description. The italicized IR mode at 284 cm^{-1} cannot be assigned to any computed one. In the *Cmcm* setting, *c* and *a* are along the leg and the rung of the ladders. The star indicates a phonon visible on the IR raw data (see Fig. 2), but that could not be properly fitted. This value is an estimation leading to larger uncertainty.

$P2_1/m$				$P2_1$			
DFT A_u	IR **E** ∥ **c**	DFT B_u	IR **E** ∥ **a**	DFT A	IR **E** ∥ **c**	DFT B	IR **E** ∥ **a**
81		87		80		87	
90		93		85		89	
104		94	96	90		92	
122	113	106		94		95	96
157		132		101		99	
181		139		104		106	
209	210	151		109	113	122	
215		184		122		130	
226		201	210	124		140	
233		233		132		151	
252	267	251		142		157	
	284	269	*266	156		181	
		280	280	179		184	
		298		187		201	
		320		204		210	210
				208	210	217	
				216		227	
				226		233	
				232		251	
				233		268	*266
				252		279	280
				255		299	
				273	267	320	
				275			
				292	284		
				315			

space group is $P2_1/m$. In this case, infrared-active modes transform as A_u and B_u. For an electric field polarized along **c** (defined with respect to the parent *Cmcm* axes), the infrared-active modes belong to the A_u representation, while for **E** ∥ **a**, they belong to the B_u representation. Raman-active modes in the $P2_1/m$ group transform as A_g and B_g. However, since our Raman measurements are performed in configurations where the incident and scattered light polarizations are parallel, only A_g modes are expected to be observed.

We also performed Raman spectroscopy at ambient temperature. As noted in previous Raman scattering studies on these samples, the signal-to-noise ratio is particularly degraded for this family of systems [29] and it worsens at high pressure due to the increased metallicity. After several attempts, we successfully measured the Raman spectra for two configurations of polarization with both the incoming and outgoing electric fields aligned along the **a** and **c** directions, respectively, corresponding to the rungs and the legs of the ladders in *Cmcm* notation.

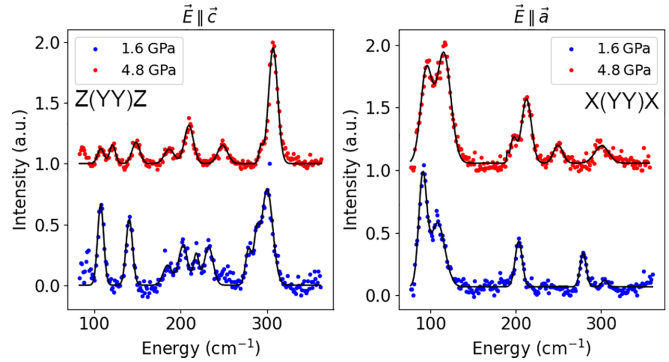

FIG. 3. Raman spectra of $BaFe_2Se_3$ at 1.6 (blue line) and 4.8 GPa (red line) at 300 K for both polarizations of the incident light [left : **E** ∥ **c** corresponding to Z(YY)Z; right: **E** ∥ **a** corresponding to X(YY)X with X,Y,Z along a,b,c in *Cmcm* setting]. They belong to the A_g irreducible representation in this configuration. The black line corresponds to the fit with Gaussian functions.

In the centrosymmetric *Cmcm* phase relevant at room temperature above 4 GPa, Raman-active phonons belong exclusively to the A_g irreducible representation in our configuration. The mutual exclusion between Raman and infrared activities is lifted in the noncentrosymmetric *Pm* phase, where phonons can be simultaneously Raman and infrared active. In this latter case, modes polarized along **c** transform as *A*, while modes polarized along **a** transform as *B*.

The Raman spectra at 1.6 and 4.8 GPa are presented in Fig. 3, together with fits using Gaussian functions for each mode. The fitted frequencies, together with their pressure evolution, are reported in the Supplemental Material [25].

Ab initio calculations. Phonons calculations were performed for both the $P2_1/m$ and $P2_1$ space groups. The structure was first relaxed under an applied pressure of 6 GPa, starting from the x-ray diffraction structural model (indeed, the 5 GPa calculations did not converge, most probably because the phase transition is close to this pressure in the DFT calculations). The frequencies of the computed lattice dynamics suggest that both structures are dynamically stable. Table I displays the DFT and experimental results in the irreducible representations (irreps) in which we have IR low-temperature measurements for comparison. The **E** ∥ **c** IR measurements correspond to the A_u irrep in the $P2_1/m$ group and *A* in the $P2_1$ group, while the **E** ∥ **a** IR measurements correspond to the B_u irrep in the $P2_1/m$ group and *B* in the $P2_1$ group.

As we can see immediately, in the $P2_1/m$ group, the phonon mode at 284 cm^{-1} for **E** ∥ **c** cannot be assigned to any computed mode, while all modes can easily be assigned in the $P2_1$ group. In fact, this mode is close in energy to two A_g modes of the $P2_1/m$ group (see the SM [25]), in agreement with the loss of the inversion center. Moreover, although it is less critical, the mode at 267 cm^{-1} for **E** ∥ **c** deviates, from the last calculated phonon at 252 cm^{-1}, further than the typical uncertainty, which is of the order of 8 cm^{-1}. Finally, despite the fact that the Raman spectra have been measured at 300 K and thus should somewhat deviate from our 0 K calculations, one can see that the mode at 197 cm^{-1} for **E** ∥ **a** cannot be associated to any computed A_g modes (see Fig. 3 and the SM [25]).

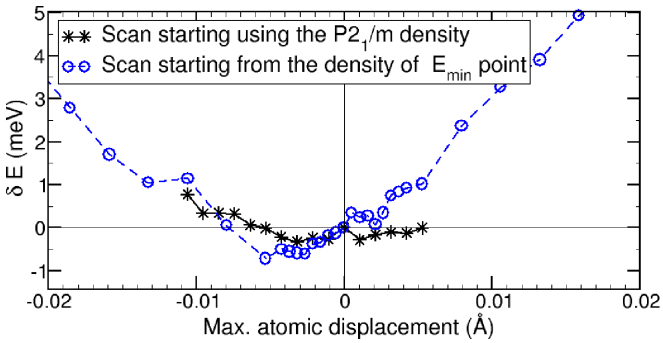

FIG. 4. Energy difference along the soft $P2_1/m$ to $P2_1$ phonons mode. The black curve uses the $P2_1/m$ density as a starting point for the self-consistent process, while the blue one uses the density of the minimum energy point of the black curve.

From all these arguments, we can reasonably conclude that the high-pressure low-temperature phase crystallizes in the $P2_1$ group.

Since the high-pressure space group $P2_1$ is not a subgroup of the ambient-pressure one Pm, the transition is expected to be first order. Of course, we cannot exclude the theoretical possibility of an intermediate phase with $P2_1/m$ symmetry in a narrow pressure range. In such a scenario, the structural evolution would proceed via two successive second-order transitions. The first-order transition senario is supported by the observation of a slight coexistence of phonon modes around 4 GPa in the $\mathbf{E} \parallel \mathbf{a}$ polarization configuration. However, this observation could also be attributed to a pressure gradient within the sample, leading to spatial phase separation and the coexistence of domains corresponding to different structures. The two-transitions scenario is supported by the flatness of the energy surface between the $P2_1/m$ and $P2_1$ structures (see Fig. 4). Although the distorted $P2_1$ structure clearly corresponds to an energy minimum, the distortion itself remains weak, with atomic displacements of the order of ∼0.005 Å, comparable to those found in spin-driven multiferroics. Moreover, even for displacements as large as 0.03 Å, the energy difference remains within a few meV. This suggests that a transition pathway involving two successive second-order transitions is, in principle, possible. Nevertheless, we consider this explanation unlikely, as the coexistence occurs over a pressure range of approximately 0.5 GPa, which exceeds the expected pressure gradient in the cell at such low pressure. In conclusion, although a multistep transition pathway cannot be ruled out, the most likely scenario remains that the structural transition is first order.

Conclusion. Through a combined experimental and theoretical approach, including x-ray diffraction, infrared and Raman spectroscopies, and *ab initio* calculations, we have determined the atomic structure of the high-pressure, low-temperature phase of $BaFe_2Se_3$ in which superconductivity emerges. Our results demonstrate that this phase crystallizes in the polar $P2_1$ space group, establishing $BaFe_2Se_3$ as a rare example of a quasi-one-dimensional noncentrosymmetric superconductor [36,37]. The absence of inversion symmetry allows, in the presence of antisymmetric spin-orbit coupling, for the mixing of spin-singlet and spin-triplet pairing channels, among other exotic phenomena [21–23,38,39]. In Fe-based systems, where the intrinsic spin-orbit coupling is moderate, such mixing is expected to be limited; nevertheless, broken inversion symmetry qualitatively alters the allowed superconducting pairing states. These findings provide a well-defined structural foundation for future investigations of superconductivity in reduced dimensionality and highlight $BaFe_2Se_3$ as a particularly promising platform for exploring the interplay between lattice symmetry, magnetism, and superconductivity in iron-based materials.

Acknowledgments. We thank SOLEIL for synchrotron beam time (Proposals No. 20210631 and No. 20220451). V.B. acknowledges the MORPHEUS platform at the Laboratoire de Physique des Solides. This work was financially supported by the ANR COCOM 20-CE30-0029, the France 2030 programme "ANR-11-IDEX-0003" via Integrative Institute of Materials from Paris-Saclay University - 2IM@UPSaclay, the Paris Ile-de-France Region in the framework of DIM MaTerRE (project DAC-VX) and by the CSC scholarship (Grant No. 201806830111) and by the CSC scholarship (Grant No. 201806830111). M.-B.L., S.D., and G.G. aknowledge the IDRIS high-performance computer center for the calculation time under the GENCI Project No. 0801842.

Data availability. The data that support the findings of this article are not publicly available upon publication because it is not technically feasible and/or the cost of preparing, depositing, and hosting the data would be prohibitive within the terms of this research project. The data are available from the authors upon reasonable request.

[1] D. J. Scalapino, A common thread: The pairing interaction for unconventional superconductors, Rev. Mod. Phys. **84**, 1383 (2012).

[2] B. Keimer, S. A. Kivelson, M. R. Norman, S. Uchida, and J. Zaanen, From quantum matter to high-temperature superconductivity in copper oxides, Nature (London) **518**, 179 (2015).

[3] G. R. Stewart, Unconventional superconductivity, Adv. Phys. **66**, 75 (2017).

[4] G. R. Stewart, Superconductivity in iron compounds, Rev. Mod. Phys. **83**, 1589 (2011).

[5] R. M. Fernandes, A. V. Chubukov, and J. Schmalian, What drives nematic order in iron-based superconductors? Nat. Phys. **10**, 97 (2014).

[6] E. Fradkin, S. A. Kivelson, and J. M. Tranquada, *Colloquium*: Theory of intertwined orders in high-temperature superconductors, Rev. Mod. Phys. **87**, 457 (2015).

[7] D. C. Johnston, The puzzle of high temperature superconductivity in layered iron pnictides and chalcogenides, Adv. Phys. **59**, 803 (2010).

[8] A. A. Kordyuk, Iron-based superconductors: Magnetism, superconductivity, and electronic structure (Review article), Low Temp. Phys. **38**, 888 (2012).

[9] V. Balédent, F. Rullier-Albenque, D. Colson, G. Monaco, and J. P. Rueff, Stability of the Fe electronic structure through temperature-, doping-, and pressure-induced transitions in the $BaFe_2As_2$ superconductors, Phys. Rev. B **86**, 235123 (2012).

[10] V. Balédent, F. Rullier-Albenque, D. Colson, J. M. Ablett, and J. P. Rueff, Electronic properties of $BaFe_2As_2$ upon doping and

pressure: The prominent role of the As *p* orbitals, Phys. Rev. Lett. **114**, 177001 (2015).

[11] H. Takahashi, A. Sugimoto, Y. Nambu, T. Yamauchi, Y. Hirata, T. Kawakami, M. Avdeev, K. Matsubayashi, F. Du, C. Kawashima, H. Soeda, S. Nakano, Y. Uwatoko, Y. Ueda, T. J. Sato, and K. Ohgushi, Pressure-induced superconductivity in the iron-based ladder material $BaFe_2S_3$, Nat. Mater. **14**, 1008 (2015).

[12] J. Ying, H. Lei, C. Petrovic, Y. Xiao, and V. V. Struzhkin, Interplay of magnetism and superconductivity in the compressed fe-ladder compound $BaFe_2S_3$, Phys. Rev. B **95**, 241109(R) (2017).

[13] H. Lei, H. Ryu, A. I. Frenkel, and C. Petrovic, Anisotropy in $BaFe_2Se_3$ single crystals with double chains of fese tetrahedra, Phys. Rev. B **84**, 214511 (2011).

[14] Y. Nambu, K. Ohgushi, S. Suzuki, F. Du, M. Avdeev, Y. Uwatoko, K. Munakata, H. Fukazawa, S. Chi, Y. Ueda, and T. J. Sato, Block magnetism coupled with local distortion in the iron-based spin-ladder compound $BaFe_2Se_3$, Phys. Rev. B **85**, 064413 (2012).

[15] M. Mourigal, S. Wu, M. B. Stone, J. R. Neilson, J. M. Caron, T. M. McQueen, and C. L. Broholm, Block magnetic excitations in the orbitally selective Mott insulator $BaFe_2Se_3$, Phys. Rev. Lett. **115**, 047401 (2015).

[16] H. Hong and H. Steinfink, The crystal chemistry of phases in the Ba-Fe-S and Se systems, J. Solid State Chem. **5**, 93 (1972).

[17] V. Svitlyk, G. Garbarino, A. D. Rosa, E. Pomjakushina, A. Krzton-Maziopa, K. Conder, M. Nunez-Regueiro, and M. Mezouar, High-pressure polymorphism of $BaFe_2S_3$, J. Phys.: Condens. Matter **31**, 085401 (2019).

[18] W.-G. Zheng, V. Baledent, C. V. Colin, F. Damay, J.-P. Rueff, A. Forget, D. Colson, and P. Foury-Leylekian, Universal stripe order as a precursor of the superconducting phase in pressurized $BaFe_2Se_3$ spin ladder, Commun. Phys. **5**, 183 (2022).

[19] W. Zheng, V. Balédent, M. B. Lepetit, P. Retailleau, E. V. Elslande, C. R. Pasquier, P. Auban-Senzier, A. Forget, D. Colson, and P. Foury-Leylekian, Room temperature polar structure and multiferroicity in $BaFe_2Se_3$, Phys. Rev. B **101**, 020101(R) (2020).

[20] M. J. Weseloh, V. Balédent, W. Zheng, M. Verseils, P. Roy, J. B. Brubach, D. Colson, A. Forget, P. Foury-Leylekian, and M.-B. Lepetit, Lattice dynamics of $BaFe_2Se_3$, J. Phys.: Condens. Matter **34**, 255402 (2022).

[21] L. P. Gor'kov and E. I. Rashba, Superconducting 2D system with lifted spin degeneracy, Phys. Rev. Lett. **87**, 037004 (2001).

[22] K. V. Samokhin, Spin susceptibility of noncentrosymmetric superconductors, Phys. Rev. B **76**, 094516 (2007).

[23] M. Smidman, M. B. Salamon, H. Q. Yuan, and D. F. Agterberg, Superconductivity and spin-orbit coupling in noncentrosymmetric materials: A review, Rep. Prog. Phys. **80**, 036501 (2017).

[24] W. G. Zheng, V. Balédent, L. Bocher, A. Forget, D. Colson, and P. Foury-Leylekian, Origin of spin-glass-like magnetic anomaly in the superconducting and multiferroic spin ladder $BaFe_2Se_3$, Phys. Rev. B **107**, 024423 (2023).

[25] See Supplemental Material at http://link.aps.org/supplemental/10.1103/jzt8-3t2c for containing results of the different x-ray diffraction refinements performed at selected pressure and temperature, a table of fitted frequencies from Raman and infrared spectroscopies, and details on the DFT calculations.

[26] A. Celeste, F. Borondics, and F. Capitani, Hydrostaticity of pressure-transmitting media for high pressure infrared spectroscopy, High Press. Res. **39**, 608 (2019).

[27] N. Tateiwa and Y. Haga, Evaluations of pressure-transmitting media for cryogenic experiments with diamond anvil cell, Rev. Sci. Instrum. **80**, 123901 (2009).

[28] G. Shen, Y. Wang, A. Dewaele, C. Wu, D. E. Fratanduono, J. Eggert, S. Klotz, K. F. Dziubek, P. Loubeyre, O. V. Fat'yanov, P. D. Asimow, T. Mashimo, and R. M. Wentzcovitch, Toward an international practical pressure scale: A proposal for an IPPS ruby gauge (IPPS-Ruby2020), High Press. Res. **40**, 299 (2020).

[29] Z. V. Popović, M. Šćepanović, N. Lazarević, M. Opačić, M. M. Radonjić, D. Tanasković, H. Lei, and C. Petrovic, Lattice dynamics of $BaFe_2X_3$ (X= S, Se) compounds, Phys. Rev. B **91**, 064303 (2015).

[30] A. D. Becke, Density-functional thermochemistry. III. The role of exact exchange, J. Chem. Phys. **98**, 5648 (1993).

[31] D. Vilela Oliveira, J. Laun, M. F. Peintinger, and T. Bredow, BSSE-correction scheme for consistent Gaussian basis sets of double-and triple-zeta valence with polarization quality for solid-state calculations, J. Comp. Chem. **40**, 2364 (2019).

[32] M. Kaupp, P. v. R. Schleyer, H. Stoll, and H. Preuss, Pseudopotential approaches to Ca, Sr, and Ba hydrides. Why are some alkaline earth MX_2 compounds bent? J. Chem. Phys. **94**, 1360 (1991).

[33] J. Heyd, J. E. Peralta, G. E. Scuseria, and R. L. Martin, Energy band gaps and lattice parameters evaluated with the Heyd-Scuseria-Ernzerhof screened hybrid functional, J. Chem. Phys. **123**, 174101 (2005).

[34] A. Erba, J. K. Desmarais, S. Casassa, B. Civalleri, L. Donà, I. J. Bush, B. Searle, L. Maschio, L. Edith-Daga, A. Cossard, C. Ribaldone, E. Ascrizzi, N. L. Marana, J.-P. Flament, and B. Kirtman, CRYSTAL23: A program for computational solid state physics and chemistry, J. Chem. Theory Comput. **19**, 6891 (2023).

[35] V. Petříček, L. Palatinus, J. Plášil, and M. Dušek, JANA2020 - a new version of the crystallographic computing system JANA, Zeitschrift fur Kristallographie - Crystalline Materials **238**, 271 (2023).

[36] J. K. Bao, J. Y. Liu, C. W. Ma, Z. H. Meng, Z. T. Tang, Y. L. Sun, H. F. Zhai, H. Jiang, H. Bai, C. M. Feng, Z. A. Xu, and G. H. Cao, Superconductivity in quasi-one-dimensional $K_2Cr_3As_3$ with significant electron correlations, Phys. Rev. X **5**, 011013 (2015).

[37] Ž Gosar, T. Arh, K. Jaksetič, A. Zorko, W. Liu, H. Wu, C. Wang, H. Luetkens, B. Lv, and D. Arčon, The pairing symmetry in quasi-one-dimensional superconductor $Rb_2Mo_3As_3$, J. Phys. Chem. Solids **181**, 111478 (2023).

[38] S. Yip, Noncentrosymmetric superconductors, Annu. Rev. Condens. Matter Phys. **5**, 15 (2014).

[39] F. Kneidinger, E. Bauer, I. Zeiringer, P. Rogl, C. Blaas-Schenner, D. Reith, and R. Podloucky, Superconductivity in noncentrosymmetric materials, Phys. C: Supercond. Appl. **514**, 388 (2015).